Support effect in supported Ni catalysts on their performance for methane partial oxidation

J. Barbero [a], M.A. Peña [a], J.M. Campos-Martin [a], J.L.G. Fierro [a], and P.L. Arias [b,*]

[a] Instituto de Catálisis y Petroleoquímica, CSIC, Cantoblanco, 28049 Madrid, Spain
[b] Escuela Superior de Ingenieros, UPV/EHU, Alameda Urquijo s/n, 48013 Bilbao, Spain

Received 18 April 2002; accepted 11 February 2003

Supported nickel catalysts were prepared by impregnation of La_2O_3, MgO and ZrO_2 substrates and tested in the partial oxidation of methane to synthesis gas at atmospheric pressure. Nickel interacted strongly with La_2O_3 forming a deficient $LaNiO_{3-\delta}$ perovskite structure upon calcination. Upon reduction at 973 K, the Ni/La_2O_3 catalysts that resulted were highly active and selective for syngas production. By contrast, a separate and readily reducible NiO phase was formed on the ZrO_2 support. Because the interaction of metallic nickel particles on ZrO_2 is weak, the catalysts underwent deactivation by sintering of metal particles during on-stream operation as confirmed by photoelectron spectroscopy. The relatively high activity of the Ni/MgO systems was associated with the formation of a highly stable cubic Ni–Mg–O solid solution, in which nickel remains highly dispersed during the methane partial oxidation reaction.

KEY WORDS: nickel; lanthana; zirconia; magnesia; catalysts; methane; partial oxidation; hydrogen.

1. Introduction

In the past few years, the partial oxidation of methane (POM) to syngas has been investigated [1–7]. The reaction is exothermic, yields H_2/CO ratios suitable for use in the production of methanol and Fischer–Tropsch synthesis, and operates at temperatures where no NO_x emissions are produced. The catalysts reported to be active in the POM reaction to syngas are either noble metals [2,3,6,7] or Ni-based catalysts [4–11]. Despite the high activity of noble metal-based catalysts for the POM reaction, the high cost of such systems limits their widespread industrial application.

Lunsford *et al.* [8] reported virtually complete CH_4 conversions and a CO selectivity of close to 95% at temperatures somewhat above 970 K on Ni/Al_2O_3 catalysts, with stable operation only if an oxygen excess above the stoichiometry of the reaction ($CH_4/O_2 < 2$) was supplied. Slagtern and Olsbye [5] studied the POM reaction on several H_2-reduced perovskite oxides and observed rapid deactivation due to the formation of large amounts of carbon deposits. Basic supports or alkali/alkaline-earth additives have been used to reduce carbon deposition on Ni catalysts. For instance, NiO–MgO solid solutions display a rather good stability in the reforming of CH_4 with CO_2 because of their pronounced basicity and high Ni dispersion [12–14]. La_2O_3 stabilizes surface carbonate structures, which act as a source of reactive oxygen species and lead to ready gasification of carbon deposits [15]. In this sense, Tsipouriari *et al.* [16] reported that the enhanced stability of Ni/La_2O_3 catalysts is related to the decoration of the metal Ni particles with a lanthanum oxy-carbonate, which favors the removal of excess carbon deposits and provides catalyst stability.

It has been observed that Ni^{2+}/Ni^{3+} ions, stabilized by solid-state reactions in oxide matrices, show a high and stable activity in POM under a high space velocity and high reaction temperature. This is mainly due to the fact that nickel ions are sparingly reduced, small Ni clusters being developed. Since coke formation requires rather large metal ensembles [17], its production is largely avoided. In addition, the metal clusters remain partially embedded in the support, which retards the sintering of metal particles [13]. In the light of the above, the aim of the present work is to provide a basic insight into the catalytic behavior of supported nickel catalysts, in which the support largely differs in basicity (La_2O_3, MgO and ZrO_2), in the POM at atmospheric pressure. The effect of Ni loading is also highlighted.

2. Experimental

2.1. Catalyst preparation

The supported nickel catalysts (Ni/La_2O_3, Ni/MgO and Ni/ZrO_2) were prepared by the wet impregnation method, using $Ni(NO_3)_2 \cdot 6H_2O$ (Aldrich-Chemie) as the metal precursor. The desired amounts of $Ni(NO_3)_2$ were dissolved in 40 mL of distilled water and then contacted with the support material, La_2O_3 (pore

* To whom correspondence should be addressed.
E-mail: iaparerp@bi.ehu.es

1011-372X/03/0400-0211/0

Table 1
Chemical analysis and specific areas of supported Ni catalysts

Support	Catalyst	Chemical analysis (wt%)				S_{BET} (m^2/g)
		Ni	La	Mg	Zr	
La_2O_3	3.9NL	3.9	65.0	–	–	6.3
	15.0NL	15.0	59.1	–	–	6.6
	25.1NL	25.1	53.6	–	–	3.4
MgO	7.7NM	7.3	–	41.0	–	8.0
	15.9NM	15.9	–	36.6	–	12.0
ZrO_2	4.4NZ	4.4	–	–	57.1	4.3
	14.5NZ	14.5	–	–	48.3	4.1

volume 0.10 cm^3/g, particle size $<100\,\mu m$, from Aldrich-Chemie), ZrO_2 (pore volume 0.09 cm^3/g, particle size $<80\,\mu m$, from MEL Chemicals, $ZrO_2 > 95.5$ wt%) and MgO (pore volume 0.14 cm^3/g, particle size $<80\,\mu m$, from Aldrich-Chemie), keeping the suspensions under continuous stirring. The water excess was evaporated off in a rotary evaporator to dryness at 353 K. The precursors were then decomposed at 623 K for 2 h, and finally calcined in air at 1173 K for 2 h. All samples were pressed (2 kbar), crushed and sieved and the 0.125–0.250 mm fraction was collected. The nickel, lanthanum, magnesium and zirconium contents, as determined by inductively coupled plasma emission spectroscopy, along with the notation used to identify the samples, are shown in table 1.

2.2. Characterization techniques

Specific areas were calculated by the BET method from the nitrogen adsorption isotherms, recorded at liquid nitrogen temperature using a Micromeritics apparatus model ASAP-2000, taking a value of 0.162 nm^2 for the cross-sectional area of the N_2 molecule adsorbed at 77 K. Prior to adsorption measurements, samples were outgassed at 413 K. The specific areas of the samples ranged from 3.4 to 12.0 m^2/g.

Powder X-ray diffraction (XRD) patterns of the precursors and calcined samples were recorded using a Seifert 3000 P diffractometer, using nickel-filtered CuKα1 ($\lambda = 0.15406$ nm) radiation. The step scans were taken over the range of 2θ angles from 20 to 70°.

A Micromeritics TPD/TPR 2900 apparatus was used for temperature-programmed reduction (TPR) analyses. Reduction profiles were obtained by passing a 10% H_2/Ar flow at a rate of 50 mL(STP)/min through the sample (weight around 30 mg). The temperature was increased from 300 to 1050 K at a rate of 10 K/min, and the amount of hydrogen consumed was determined as a function of temperature. Under these conditions, line profile and peak positions can be accurately measured.

X-ray photoelectron spectra (XPS) were acquired with a VG Escalab 200R spectrometer equipped with a hemispherical electron analyzer and an AlKα1 ($h\nu = 1486.6$ eV, 1 eV = 1.6302×10^{-19} J) X-ray source. The powder samples were reduced *ex situ* in H_2 at 1073 K for 1 h in a flow system and then collected in isooctane before being transferred to the pretreatment chamber of the spectrometer. Peak intensities were estimated by calculating the integral of each peak, after smoothing, subtraction of the S-shaped background, and fitting the experimental curve to a combination of Lorentzian and Gaussian lines. All binding energies (BE) were referred to the C 1*s* line at 284.9 eV, which afforded BE value estimation with an accuracy of ±0.1 eV.

2.3. Catalytic activity

The catalytic oxidation of methane was carried out in a fixed-bed quartz tubular reactor (9 mm i.d.) at atmospheric pressure. Catalyst particles (20–60 mg; 0.125–0.25 mm) were diluted with SiC (SiC/catalyst = 2) to reduce the volumetric heat release and were placed between quartz-wool swatches in the middle of the reactor. The temperature of the catalytic bed was monitored by a chromel–alumel thermocouple, protected with a 4 mm diameter quartz sleeve, placed in the catalyst bed center. Prior to catalytic tests, the catalysts were reduced in a H_2 stream at 973 K followed by purging in a He stream, while fixing the starting reaction temperature, typically 773 K. The reaction mixture was fed by mass-flow controllers (Brooks 5850) at a total flow rate of 30–90 mL(STP)/min with molar ratio of $N_2:CH_4:O_2 = 3:2:1$. Catalytic runs were extended for periods of 6–8 h, always in increasing order of temperature. Blank runs were conducted with an empty reactor without any detectable conversion. Product analysis was accomplished using an on-line gas chromatograph (HP-5890) provided with a TC detector, and Porapak N- and molecular sieve 5A-packed columns, using helium as carrier gas.

3. Results and discussion

3.1. X-ray diffraction

The crystal structures of NL, NM and NZ catalysts calcined at 1173 K was revealed by XRD. Figure 1(a) shows XRD patterns of two representative catalysts (3.9NL and 15.0NL) and also that of the support. As judged from its pattern, the support is completely hydrated and peaks belonging to $La(OH)_3$ are observed (rhombohedral system, spatial group P6 3/m, parameters $a = 6.5286$ and $b = 3.8588$ Å). For the NL catalysts with Ni loadings below 15%, the diffraction lines of the $La(OH)_3$ phase are accompanied by that of a La_2NiO_4 phase (tetragonal system, spatial group I4/m, parameters $a = 3.855$ and $b = 16.652$ Å). As $La(OH)_3$ phase was

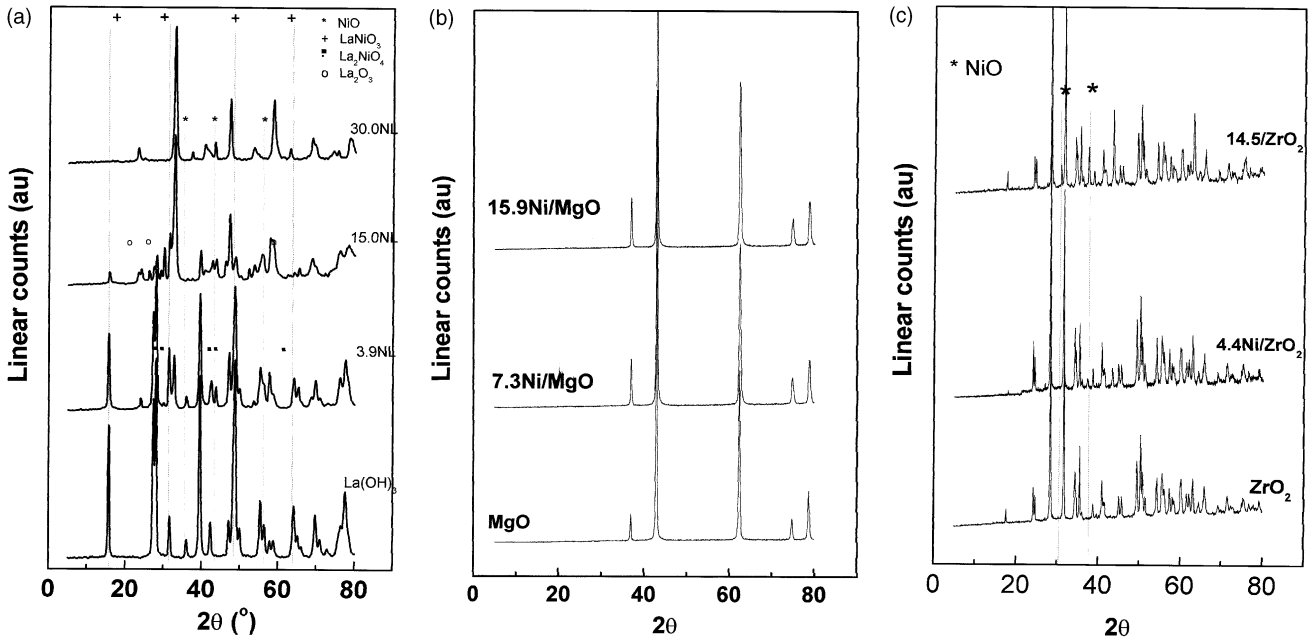

Figure 1. XRD patterns of calcined catalysts at 1173 K. (a) NL samples. For the sake of comparison, the XRD pattern of an $La(OH)_3$ reference is included. (b) NM samples. (c) NZ samples. Symbols for phase identification are indicated.

observed, it is inferred that water uptake might have happened between calcination and XRD measurements. However, for catalysts with Ni loadings of 15.0% and above diffraction lines at Bragg angles of *ca.* 23, 47 and 59° are observed. These new diffraction lines are indexed to the $LaNiO_3$ perovskite phase (rhombohedral system, spatial group R, parameters $a = 5.451$ and $b = 6.564$ Å) [18]. For the catalyst 15.0NL, nickel is incorporated into the $LaNiO_3$ phase while part of the lanthanum remains as a La_2O_3 phase (hexagonal system, spatial group P321, parameters $a = 3.93$ and $b = 6.12$ Å). For the 25.1NL catalyst nickel is distributed inside the $LaNiO_3$ but also in the NiO phase (rhombohedral system, spatial group R-3m, parameters $a = 2.9552$ and $b = 7.2275$ Å).

The XRD patterns of NM catalysts were quite simple. The diffraction lines of NM catalysts virtually coincided with those of the MgO (cubic system, spatial group Fm3m, parameter $a = 4.209$ Å) phase and no other lines of Ni-containing phases were discerned (figure 1(b)). Although the (Mg,Ni)O system tends to develop the $MgNiO_2$ (cubic system, spatial group Fm3m, parameter $a = 4.1922$ Å) phase, its symmetry and unit cell parameter are essentially the same as for the MgO substrate. Thus, the XRD technique does not permit one to distinguish between the Ni-containing phase and the MgO substrate. The diffraction profiles of NZ catalysts exhibited the lines of the ZrO_2 support (cubic system, spatial group $P4_2/nmc$, parameter $a = 3.5924$ Å) together with that of the NiO phase (figure 1(c)). The intensity of the diffraction lines of the NiO phase increased with increasing Ni content.

3.2. Temperature-programmed reduction

The TPR profiles of several NL, NM and NZ catalysts calcined at 1173 K are presented in figure 2. Two reduction peaks at 625 and 760 K were observed for the 25.1NL catalyst (figure 2(a)). Both peaks shift slightly to lower temperature in catalysts 15.0NL and 3.9NL, in which the Ni content is lower. Consistent with the XRD data, these peaks are due to a two-step reduction process of the $LaNiO_3$ perovskite structure [19] formed upon calcination of precursors:

$$LaNiO_3 + H_2 \rightarrow LaNiO_{3-y} + H_2O \quad \text{(low-temperature peak)} \quad (1)$$

$$LaNiO_{3-y} + H_2 \rightarrow La_2O_3 + Ni + H_2O \quad \text{(high-temperature peak)}. \quad (2)$$

$LaNiO_{3-y}$ are deficient perovskites, in which the oxygen non-stoichiometry is accommodated by disordered intergrowth of octahedral and square-planar layers along the $[100]_c$ face [20]. These non-stoichiometric compounds stabilize Ni^{2+} and Ni^{+} oxidation states, which account for an incomplete reduction. The TPR profiles of the 15.0NL and 3.9NL samples are more complex and a third peak located at *ca.* 845 K can be distinguished. As stated above, these two samples exhibited a La_2NiO_4 phase, which was dominant in the 3.9NL sample. Since the intensity of the TPR peak is higher for the 3.9 NL sample, the peak can tentatively be assigned to the reduction of the non-stoichiometric Ni phases produced in the reduction of the La_2NiO_4 precursor.

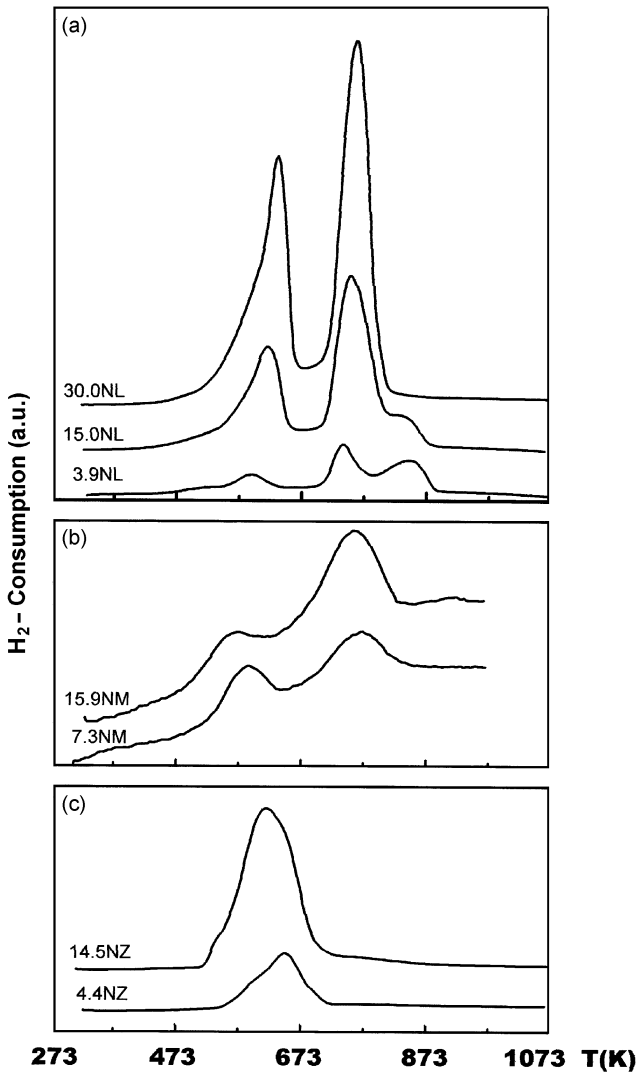

Figure 2. TPR profiles of catalysts calcined at 1173 K. (a) NL samples; (b) NM samples; (c) NZ samples. The numerals in labels refer to Ni loading.

The TPR profiles of the 7.7NM and 15.9NM catalysts are shown in figure 2(b). The profile of the 7.7NM sample displays two peaks at *ca.* 573 and 770 K, and these are shifted by 10–15 K to lower temperatures in the 15.9NM sample. Interestingly, the area underneath the TPR curve corresponding to the low-temperature peak is quite similar for both samples, but that of the high-temperature peak is nearly three-fold higher for the 15.9NM sample than for the 7.7NM counterpart. Regarding the NM catalysts, for which only diffraction peaks of the MgO phase are observed, the low-temperature TPR peak is associated with a highly dispersed NiO phase (undetected by XRD). In agreement with the work of Ruckenstein and Wang [21] on magnesia-supported cobalt catalysts, the high-temperature peak is associated with the reduction of a solid solution (Mg–Ni–O), which is developed upon calcination of the precursor at 1173 K. Unfortunately, no support in favor of this interpretation can be obtained from XRD because the diffraction patterns of the MgO support and of the Mg–Ni–O solid solutions virtually coincide.

Also included in figure 2 are the profiles of the 4.4NZ and 14.5NZ samples (figure 2(c)). Both profiles are relatively simple since they exhibit a single reduction peak at low temperature (*ca.* 655 K). Since in this catalyst series the XRD data revealed the formation of a NiO phase (cf. figure 1(c)), the observed TPR peak must be related to the reduction of a crystalline NiO phase deposited on the surface of ZrO_2. H_2 consumptions up to 973 K for the catalysts of the NZ series indicate that Ni reduction is quantitative. However, reduction is partial for NL and NM series, and its extent increased with Ni content (80% for 15.0 NL and 66% for 15.9 NM).

3.3. X-ray photoelectron spectroscopy

Prior to analysis the catalysts were reduced in the TPR equipment at 1073 K and then transferred to the pre-treatment chamber of the electron spectrometer under isooctane. The binding energies of Mg 2*p*, Zr $3d_{5/2}$, La $3d_{5/2}$ and Ni $2p_{3/2}$ core levels and surface atomic ratios are compiled in table 2. For the NL catalysts, the analysis of the Ni $2p_{3/2}$ profile was complicated, due to overlapping of the Ni $2p_{3/2}$ and La $3d_{3/2}$ peaks. The most intense Ni $2p_{3/2}$ peak, which appeared somewhat above 856 eV, is characteristic of Ni^{2+}/Ni^{3+} ions in an oxygen environment [22]. This peak was accompanied by a satellite line positioned at *ca.* 6 eV higher BE. The Ni 2*p* peaks are complicated by the simultaneous presence of the La $3d_{3/2}$ component at *ca.* 4 eV lower BE, and also by the splitting (*ca.* 4.3 eV) of the La $3d_{5/2}$ peak into two components [23]. Thus, the higher BE contribution of the La $3d_{3/2}$ peak overlaps with the Ni $2p_{3/2}$ peak. To overcome this complication, the Ni $2p_{3/2}$ + La $3d_{3/2}$ energy region was fitted to four components in decreasing BE: a shake-up satellite of Ni^{2+}, the principal Ni $2p_{3/2}$ and the two split La $3d_{3/2}$ components. The procedure appears to be reasonably accurate since the estimated error in duplicate measurements did not exceed 17%.

The Ni $2p_{3/2}$ binding energies for NL and NM (table 2) are much higher than those expected for Ni metal and typical of Ni^{2+}/Ni^{3+} species. This observation indicates that Ni^0 becomes oxidized on both the La_2O_3 and MgO

Table 2
Binding energy (eV) of core levels and surface atomic ratios of supported Ni catalysts pre-reduced in H_2 at 1073 K

Catalyst	La $3d_{5/2}$	Mg 2*p*	Zr $3d_{5/2}$	Ni $2p_{3/2}$	Ni/sup atom [a]
15.0NL	835.3	–	–	856.2	0.634
15.9NM	–	50.4	–	852.6 (27); 855.5 (73)	0.163
14.5NZ	–	–	182.2	852.5 (64); 855.6 (36)	0.703

[a] "Sup" refers to La, Mg or Zr; numbers in parentheses are peak percentages.

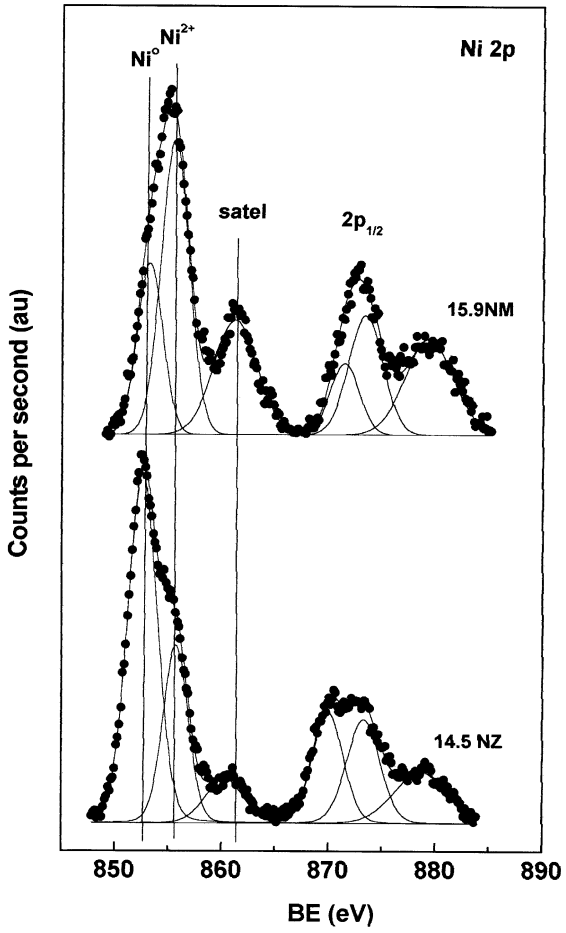

Figure 3. Photoelectron spectra of the representative 15.9NM and 14.5NZ supported Ni catalysts pre-reduced *ex situ* in hydrogen at 1073 K for 1 h.

substrates. Identical behavior has been already observed on pre-reduced $LnCoO_3$ (Ln = lanthanide) [24], in which a Co^0 metal phase was observed only for the members of the series having a less basic lanthanide but in no case for La. The appearance of Ni^{3+}/Ni^{2+} species appears to be related to the oxidizing power of surface hydroxyl groups, according to equation:

$$Ni^0 + La(OH)_3 \rightarrow LaNiO_3 + \tfrac{3}{2}H_2. \qquad (3)$$

Further support for this mechanism on NL catalysts comes from the binding energies of La $3d_{5/2}$ core level, which are similar to that measured for $La(OH)_3$ and higher than that of La_2O_3 [25]. In addition, the reduced NL and NM catalysts showed a high binding energy C 1*s* component (*ca.* 289.5 eV) due to carbonate species produced by the reaction of ambient CO_2 with the basic MgO and La_2O_3 supports.

Unlike the NL and NM catalysts, reduced NZ samples displayed the Ni $2p_{3/2}$ component of metallic Ni^0 together with a second peak due to some remaining non-reduced Ni^{2+} species (figure 3). It was also noted that the binding energy of the reduced Ni^0 phase in the 4.4NZ catalyst was substantially higher than in its 14.5NZ counterpart. This phenomenon is characteristic of very small Ni particles interacting with the substrate. Finally, from the intensities of the La $3d_{5/2}$, Mg 2*p*, Zr 3*d* and Ni $2p_{3/2}$ peaks, and considering the sensitivity factors given by Briggs *et al.* [26], the Ni/La, Ni/Mg and Ni/Zr atomic ratios were calculated. These ratios are also shown in table 2. No measurement of the Ni $2p_{3/2}$ signal was made for the 3.9NL sample because its intensity was extremely low and overshadowed by that of the La $3d_{3/2}$ component. The Ni/La ratio for the 15.0NL sample was very high. The Ni/Mg ratio was rather low for the 15.9NM samples as compared with the 15.0NL and 14.5NZ counterparts, which is consistent with the formation of a Mg–Ni–O solid solution [12,27].

3.4. Catalytic activity

First, a blank experiment with the reactor filled with SiC, of the same particle size as the catalyst, was performed by feeding a $N_2:CH_4:O_2 = 3:2:1$ (molar) gas mixture at 1073 K at atmospheric pressure. The experiment was extended for a period of 6–8 h by starting with the lowest flow rate ($GHSV = 3.6 \times 10^4/h$) and ending with the highest one ($GHSV = 1.7 \times 10^5/h$). CH_4 conversion was below 3%, decreased drastically upon increasing the GHSV, and vanished for GHSV values above $7.2 \times 10^4/h$. CO and H_2 were the major products observed, the CO/H_2 ratio remaining almost constant (*ca.* 1.8) for the range of GHSV values explored, and only small amounts of CO_2 being generated.

Table 3 shows the methane conversion and product distribution data in the POM reaction at 1073 K and a GHSV of $3.6 \times 10^4/h$ for the different catalysts. These data clearly show that the catalytic behavior strongly depends on both the Ni loading and type of support. For each family of catalysts, CH_4 conversion increased with the Ni loading and this increase was much more marked in the NM and NZ catalysts. In the low-Ni-content catalysts, this is a consequence of the much higher CH_4 conversion on the 3.9NL catalyst than on the 7.3NM and 4.4NZ counterparts. The activity order for low Ni loading was: 3.9NL $\gg$ 7.3NM $>$ 4.4NZ.

Table 3
CH_4 conversion and product distributions in the POM reaction over different catalysts

Catalyst	GHSV (h^{-1})	CH_4 conv. (%)	Selectivity (%)			
			H_2	CO	CO_2	C_{2+}
3.9NL	250	43	54	56	43	1
15.0NL	250	85	90	90	7	3
7.3NM	250	16	9	10	67	23
15.9NM	250	63	73	78	16	6
4.4NZ	250	4	0	25	75	0
14.5NZ	250	63	72	75	17	8

Note: Reaction conditions: temperature, 1073 K; atmospheric pressure; feed, $N_2:CH_4:O_2 = 3:2:1$ (molar).

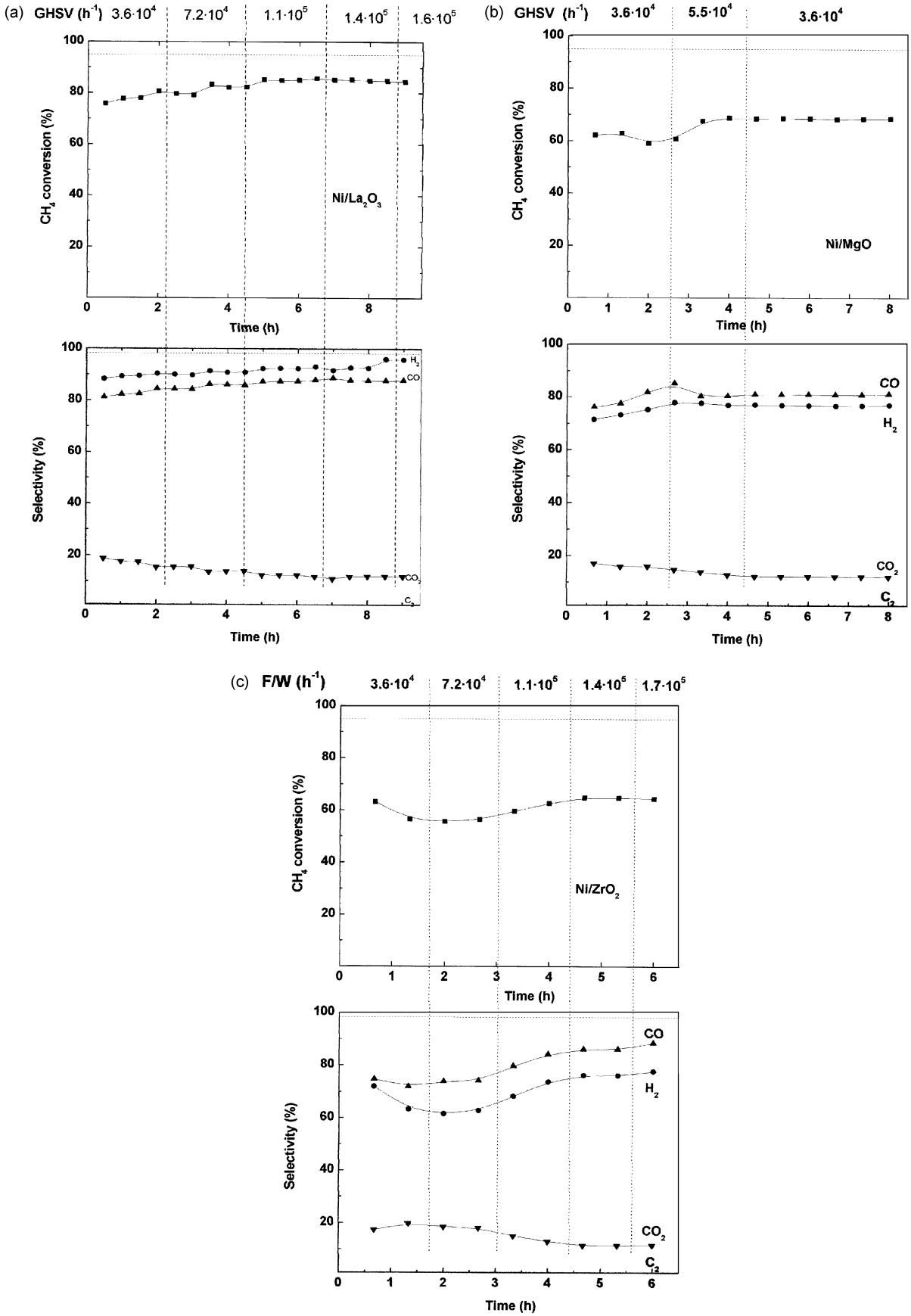

Figure 4. Effect of GHSV on the partial oxidation of CH_4. Reaction conditions: temperature, 1073 K; atmospheric pressure; feed, $N_2 : CH_4 : O_2 = 3 : 2 : 1$ (molar). (a) 15.0NL; (b) 15.9NM; (c) 14.5NZ.

However, differences in activity were less marked in the catalysts containing high Ni loadings, although the 15.0NL catalyst was still the most active. For high Ni loading, the activity order was: 15.0NL > 15.9NM ≈ 14.5NZ.

The product distribution was also strongly influenced by Ni content and also by the kind of support. At low Ni loading, the greatest H_2 selectivity was found in the 3.9NL catalyst but much lower than that expected from thermodynamic equilibrium calculations. H_2 (and CO) selectivity follows the order: 3.9NL ≫ 7.3NM > 4.4NZ. The 4.4NZ catalyst shows no H_2 formation, CO and CO_2 being the only C-containing products. This finding indicates that in the low-Ni-loading catalyst (4.4NZ), and hence with low Ni coverage, the major Ni-free ZrO_2 surface basically acts in the CH_4 combustion and dimerization reactions. Dimerization products are formed to a significant extent on the 7.3NM catalyst (23% selectivity). By contrast, in the high-Ni-content catalyst (14.5NZ), in which a highly Ni-covered ZrO_2 surface is expected to occur, partial oxidation is the dominant reaction.

The effect of GHSV on both CH_4 conversion and product distributions was studied in the high-Ni-content catalysts. CH_4 conversion was found to increase slightly with GHSV over the 15.0NL catalyst. As shown in figure 4(a), CH_4 conversion reaches a value of *ca.* 79% on the 15.0NL catalyst for a GHSV of 3.6×10^4/h, and increases slightly with the GHSV up to a plateau for a GHSV of 1.4×10^5/h. For this catalyst, selectivities to H_2 and CO followed a similar trend and approached those of the thermodynamic equilibrium. On the contrary, CO_2 selectivity decreased slightly upon increasing GHSV. For the 15.9NM catalyst, CH_4 conversion was lower (*ca.* 62%) than for the 15.0NL at a GHSV in the range 3.6×10^4–5.5×10^4/h (figure 4(b)). Once this catalyst had been tested under a GHSV of 5.5×10^4/h, the starting GHSV of 3.6×10^4/h was fixed again in order to see whether the system was reversible. It was observed that both CH_4 and the selectivities towards H_2 and CO were slightly higher than in the fresh 15.9NM catalyst. This indicates that the active phase changes during on-stream operation. Since the temperature of the catalyst bed increased slightly with the increase in GHSV up to 5.5×10^4/h, it is possible that the nickel phase could have undergone some changes during operation. It is known that Ni deposited on a MgO substrate develops, upon calcination, an Ni–Mg–O solid solution [12,27]. The cubic Ni–Mg–O solid solution is very stable, resulting in a slow migration of Ni species from the bulk to the surface during the reaction, followed by the formation of dispersed Ni metal particles, which are active and selective in the methane partial oxidation reaction.

The effect of GHSV on the behavior of the 14.5NZ catalyst was slightly different (figure 4(c)). For a GHSV of 3.6×10^4/h the initial CH_4 conversion (*ca.* 63%) decreased slightly in the first 2 h on-stream. Upon increasing the GHSV up to 7.2×10^4/h, methane conversion and selectivities towards H_2 and CO remained almost constant. However, a further increase in the GHSV led to an increase in CH_4 conversion and H_2 and CO selectivities, a constant level being reached for a GHSV of 1.4×10^5/h. By photoelectron spectroscopy it was observed not only that the Ni/Zr surface ratio of the used catalyst decreased by 6.7% with respect the fresh counterpart but also that no significant amounts of coke were deposited on the surface of the used catalyst. In addition, taking into account that the nickel precursor was readily reduced during the activation process, the interaction of the metallic phase on the ZrO_2 surface was rather weak. Both observations point to the sintering of Ni metallic particles as the most probable reason for the deactivation of the 14.5NZ catalyst.

5. Conclusion

Ni/La_2O_3 catalyst precursors activated in H_2 proved to be highly active and selective for the partial oxidation of CH_4 into synthesis gas, even at high space velocity. The TPR profiles revealed a two-step reduction process that was consistent with the formation of a deficient $LaNiO_{3-\delta}$ perovskite structure upon calcination. These mixed oxides become reduced upon activation in a hydrogen flow or under stream operation and the finely dispersed Ni metal phase in close contact with the La_2O_3 matrix produced appears to be responsible for the excellent catalytic behavior. By contrast, the Ni/ZrO_2 catalysts are readily reduced and the interaction of the metallic Ni particles with the ZrO_2 surface is too weak to stabilize the metal particles. Thus, the Ni/ZrO_2 catalysts became deactivated by sintering of metal particles upon operation, as confirmed by XPS. Finally, in the Ni/MgO systems the cubic Ni–Mg–O solid solution is very stable and displays an intermediate behavior.

Acknowledgments

The Basque Government and the industrial companies Praxair and Sociedad de Gas de Euskadi S.A. are acknowledged for supporting this research.

References

[1] P.D.F. Vernon, M.L.H. Green, A.K. Cheetham and A.T. Ashcroft, Catal. Lett. 6 (1990) 181.
[2] D.A. Hickman and L.D. Schmidt, J. Catal. 138 (1992) 267.
[3] D.A. Hickman, E.A. Hanpfear and L.D. Schmidt, Catal. Lett. 17 (1993) 223.
[4] J.B. Claridge, M.L.H. Green, S.C. Tsang, A.P.E. York, A.T. Ashcroft and P.D. Battle, Catal. Lett. 22 (1993) 299.
[5] A. Slagtern and U. Olsbye, Appl. Catal. A: General 110 (1994) 99.

[6] E.P.J. Mallens, J.H.B.J. Hoebnik and G.B. Marin, Catal. Lett. 33 (1995) 291.
[7] M.A. Peña, J.P. Gomez and J.L.G. Fierro, Appl. Catal. A: General 144 (1996) 7.
[8] D. Dissanayake, M.P. Rosynek, K.C.C. Kharas and J.H. Lunsford, J. Catal. 132 (1991) 117.
[9] Y.H. Hu and E. Ruckenstein, J. Catal. 158 (1996) 260.
[10] Y. Chu, S. Li, J. Lin, J. Guo and Y. Yang, Appl. Catal. A: General 134 (1996) 67.
[11] V.R. Choudhary, B.S. Uphade and A.A. Belhekar, J. Catal. 163 (1996) 312.
[12] O. Yamazaki, K. Tomishige and K. Fujimoto, Appl. Catal. A: General 136 (1996) 49.
[13] E. Ruckenstein and Y.H. Hu, Appl. Catal. A: General 133 (1995) 149.
[14] K. Tomishige, Y. Chen and K. Fujimoto, J. Catal. 181 (1999) 91.
[15] A. Slagtern, Y. Schuurman, C. Leclercq, X. Verykios and C. Mirodatos, J. Catal. 172 (1997) 118.
[16] V.A. Tsipourari, Z. Zhang and X.E. Verykios, J. Catal. 179 (1998) 283.
[17] J.R. Rostrup-Nielsen, in: *Catalysis Science and Technology*, Vol. 5, eds. J.R. Anderson and M. Boudart (Springer Verlag, Berlin, 1984) p. 118.
[18] J.L.G. Fierro and L.G. Tejuca, J. Catal. 87 (1984) 126.
[19] M.A. Peña and J.L.G. Fierro, Chem. Rev. 101 (2001) 1981.
[20] M.J. Sayagues, M. Vallet-Regí, A. Caneiro and J.M. Gonzalez-Calbet, J. Solid State Chem. 110 (1994) 295.
[21] E. Ruckenstein and H.Y. Wang, Catal. Lett. 70 (2000) 15.
[22] S. Damyanova, L. Daza and J.L.G. Fierro, J. Catal. 159 (1996) 150.
[23] L.P. Haack, C.R. Peters, J.E. Vriesand and K. Otto, Appl. Catal. A: General 87 (1992) 103.
[24] R. Lago, G. Bini, M.A. Peña and J.L.G. Fierro, J. Catal. 167 (1997) 198.
[25] J.S. Ledford, M. Houalla, A. Proctor and D.M. Hercules, J. Phys. Chem. 93 (1989) 6770.
[26] D. Briggs and M.P. Seah, eds., *Practical Surface Analysis by Auger and and X-Ray Photoelectron Spectroscopy*, 2nd ed. (Wiley, Chichester, 1990).
[27] F. Arena, F. Frusteri, A. Parmaliana, L. Plyasova and A.N. Shmakov, J. Chem. Soc., Faraday Trans. 92 (1996) 469.